CTSMA: Cyclic Time Shift Multiple Access for Underwater Acoustic Networks

Zhile Li, Zhuoran Qi, Dario Pompili
Department of Electrical and Computer Engineering, Rutgers University–New Brunswick, NJ, USA
Emails: {*zhile.li, zhuoran.qi, pompili*}*@rutgers.edu*

2024 IEEE 21st International Conference on Mobile Ad-Hoc and Smart Systems (MASS) | 979-8-3503-6399-9/24/$31.00 ©2024 IEEE | DOI: 10.1109/MASS62177.2024.00043

***Abstract*—Reliable and efficient underwater communication techniques are crucial and urgently needed in the underwater Internet of Things (UW IoT), and it is challenging due to the harsh conditions of the underwater channel. Furthermore, an effective and underwater acoustic-specific Medium Access Control (MAC) layer protocol is necessary for a multi-user network, such as Wireless Sensor Networks (WSN) or fleet of Autonomous Underwater Vehicles (AUVs). To address these challenges, a novel cross-layer scheme has been proposed that integrates the physical layer and the MAC layer, termed Cyclic Time Shift Multiple Access (CTSMA). CTSMA enables multiple users to transmit and receive different data streams within the same network, by using specialized Zero-Correlation-Zone (ZCZ) sequence division. The performance of this framework has been investigated and validated through both emulations and tank experiments with our custom-made underwater IoT devices. The results demonstrate that CTSMA offers superior transmission accuracy than chaotic code-based Code Division Multiple Access (CDMA) under the same coding rate condition.**

I. Introduction

Recent advances in underwater wireless communication networks have garnered significant interest, primarily due to their vital applications in the military, commercial, and scientific sectors [1]. In particular, the concept of the Underwater Internet of Things (UW IoT) has enabled a wide variety of practical applications in aquatic environments. These applications include oceanographic data collection, environmental and pollution monitoring, tsunami detection and disaster mitigation, assisted navigation, and strategic surveillance [2]–[4]. Therefore, establishing an effective and reliable communication protocol that encompasses both the Physical (PHY) layer and the Medium Access Control (MAC) layer is essential for the realization of a UW IoT network. However, underwater wireless communication faces significant challenges due to the unpredictable nature of underwater environments.

In the vast underwater environment, three distinct wireless communication methods have been considered: (i) optical waves, (ii) radio frequency, and (iii) acoustic waves. Among these, optical waves offer a wide bandwidth of hundreds of MHz and data rates in the Gbps range, with coverage distances of up to $100\ \mathrm{m}$ [5]–[7]. However, optical waves face attenuation issues due to absorption, scattering, and reflection by suspended particles in water. In addition, interference from solar background noise hampers optical performance in shallow water and during daylight operations. The radio frequency operates within a bandwidth of several MHz, achieving data rates of up to $100\ \mathrm{Mbps}$ [8]. Widely used for short-range communications in shallow water, radio frequency encounters challenges due to high attenuation in seawater caused by its high conductivity and permittivity. Consequently, its coverage range is limited to approximately $10\ \mathrm{m}$.

In this context, the use of acoustic waves emerges as the most viable option for medium/long-range underwater wireless communications, which achieves a coverage distance of kilometres [9], [10]. However, the underwater acoustic channel is susceptible to limited bandwidth and multipath effects. The slow speed of sound in water also results in significant propagation delays and Doppler effects. Despite these obstacles, technologies rooted in acoustic wave-based communication offer a promising method for enabling underwater transmission. Furthermore, the characteristic of acoustic communication broadcast is also suitable for specific applications, such as the coordination of fleets of Autonomous Underwater Vehicles (AUVs) and sensing data collection among a wireless sensor network.

In addition to the above challenges of the PHY layer, commonly used terrestrial multiple access techniques are unsuitable for underwater environments due to various limitations. These limitations include high power consumption, computational complexity, limited bandwidth, and propagation delays. Consequently, a task-specific integration framework for Underwater Acoustic Communications (UAC) is essential to devise innovative solutions that effectively address these challenges.

Our Vision: Fig. 1 depicts our vision for the UW IoT, where the PHY layer and the MAC layer communication can be achieved by the small-size on-board modem that is implemented in all objects. To address the above challenges and realize our goals, three main objectives need to be fulfilled: (i) Task-specific to UACs – the capability to resist signal selective fading and strong multipath in harsh channels; (ii) Low energy consumption – prevent high complexity schemes, and also avoid the solutions with high Peak-to-Average Power Ratio (PAPR) transmission power, which will introduce nonlinear distortion and impact performance of the front-end circuit in IoT modems; (iii) An efficient and reliable MAC layer protocol for multiuser/multinode application scenarios.

Contributions: In this work, we propose a novel integration layer framework for underwater acoustic networks and validate performance in emulations and tank experiments. The contributions are as follows.

2155-6814/24/$31.00 ©2024 IEEE
DOI 10.1109/MASS62177.2024.00043

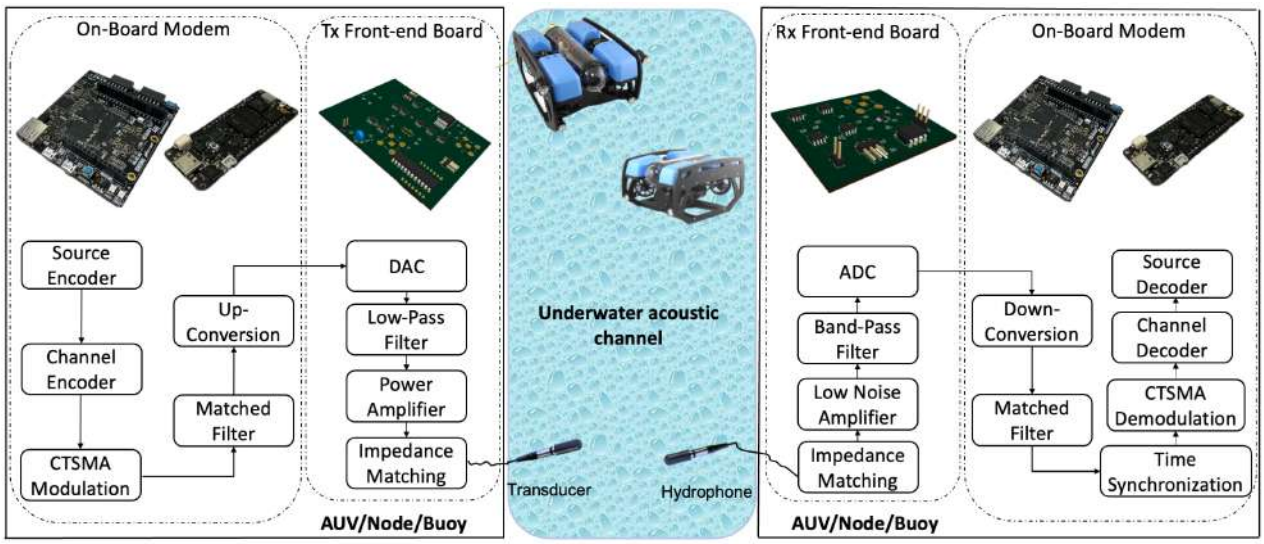

Fig. 1: High-level architecture for envisioning UW IoT, with multiple AUVs and underwater sensing nodes in a communication network. The two boxes on the left and right are the on-board modem with the front-end circuit, which are of the size of a credit card and are implemented inside the AUVs and nodes. All digital processing, including CTSMA modulation, is implemented in the Field Programmable Gate Array (FPGA) or Microcontroller (MCU). In the MAC layer, they are designed to simultaneously transmit messages to any user within the network in the same frequency band.

- We propose a novel MAC layer strategy, integrating the PHY layer and the MAC layer using Cyclic Time Shift Multiple Access (CTSMA) sequences for every user.
- We provide a comprehensive derivation of the equations for the CTSMA modulation and demodulation, which utilizes the high autocorrelation and low cross-correlation of ZCZ sequences.
- We evaluated the performance of our proposed CTSMA scheme by comparing it with chaotic code-based Code Division Multiple Access (CDMA) through emulations. These emulations are based on real channels collected from at-sea experiments conducted at Barnegat Bay, New Jersey. Subsequently, we presented and analyzed the performance metrics of Bit Error Rate (BER) and spectral efficiency.
- We conducted tank experiments using two transducers and one hydrophone, along with our custom-made underwater acoustic front-end circuitry in both the transmitter and receiver. Additionally, we utilize Software-Defined Radio (SDR) devices for our setup. Both the simulation and experiment results show the reliability and feasibility of our proposed CTSMA.

Paper Outline: In Section II, we go over the state-of-the-art and related research in the literature. In Section III, we discuss our proposed work, including perspectives both on the PHY layer and on the MAC layer. In Section IV, we first present the results of the emulation and discuss the benefits of our solution, then bring our work to the tank experiment. Finally, in Section V, we draw conclusions and discuss future work.

II. Related Work

The emergence of Underwater IoT (UIoT) has garnered significant attention in recent years [11], stimulating research across various related domains, including research on underwater unmanned vehicles [12], underwater wireless sensor networks [13] and marine science [14]. In [15], we propose a new low-power and environmentally friendly underwater data acquisition solution, which leverages Analog Joint Source-Channel Coding (AJSCC) [16] and correlation-aware Hybrid Automatic Repeat Request (HARQ) [17], providing a framework for underwater WSNs that minimize retransmissions and conserve energy and time.

In the PHY layer, coherent modulations such as Phase Shift Keying (PSK) and Quadrature Amplitude Modulation (QAM) typically offer higher spectral efficiency than non-coherent modulation schemes like differential PSK and M-ary Frequency Shift Keying (MFSK) [18]. However, coherent detection, necessary for coherent demodulation, significantly increases complexity and may not be suitable for underwater IoT devices. Pulse Position Modulation (PPM) provides a noncoherent alternative and has demonstrated robustness against thermal noise and channel attenuation [19]. However, it is sensitive to multipath delays resulting from reflection and scattering, which can severely impact the demodulation performance if the power of multipath delay signals plus additive noise exceeds Line Of Sight (LOS) [20]. Orthogonal Frequency Division Multiplexing (OFDM) is widely employed in both terrestrial and underwater wireless communication due to its potential against multipath effects, facilitated by pilot signal insertion [5].

However, its elevated PAPR poses limitations on its application in underwater IoT devices. The energy-constrained operational amplifier (Op-Amp) struggles to amplify the transmission signal without distortion. An alternative approach to OFDM, termed Orthogonal Signal Division Multiplexing (OSDM), has been proposed in [21], achieving lower PAPR. However, the high-complexity algorithm associated with OSDM makes it unsuitable for IoT devices. In our previous work [22], [23], we developed a nonlinear and noncoherent modulation scheme known as Circular Time Shift Modulation (CTSM). CTSM offers a higher robustness of the system against UAC channel interference and additive noise compared to PPM, making it a promising candidate for underwater IoT applications.

In the MAC layer, a reliable and efficient protocol is crucial, especially in the context of underwater IoT. Previous studies [24] have explored ALOHA-based protocols designed to exploit the characteristics of acoustic waves, resulting in improvements in collision reduction and transmission efficiency. Time Division Multiple Access (TDMA) [25] and Frequency Division Multiple Access (FDMA) [26] encounter challenges such as propagation delay, limited bandwidth, and fading in time and frequency fading due to multipath and Doppler effects. Carrier Sense Multiple Access with Collision Avoidance (CSMA/CA) [27] is a MAC protocol commonly used for packet traffic management in wireless networks, particularly in IEEE 802.11 wireless Local-Area Networks (LAN). However, continuous carrier monitoring is impractical for power-constrained devices.

Orthogonal Frequency Division Multiple Access (OFDMA) [28] allocates orthogonal subcarriers to different users, allowing simultaneous data transmission and reception in the same frequency band. However, the high PAPR in OFDMA can distort linear devices such as power amplifiers. Moreover, the narrow bandwidth in UAC restricts the application of OFDMA. Code Division Multiple Access (CDMA) [29], [30] assigns orthogonal CTSMA sequences to different users, offering a promising solution despite relatively low throughput and the requirement for coherent detection. In our previous studies [31], [32], experiments are carried out in UAC multicast networks based on CDMA, OFDM, and OSDM, with one user transmitting and two or three users receiving. Furthermore, we proposed Orthogonal Signal Division Multiple Access (OSDMA) in [33], which allocates different Inverse Digital Fourier Transform (IDFT) sequences to different users. Emulations are performed with one user transmitting and two users receiving. Given the necessity of establishing a reliable underwater acoustic network, we believe that our proposed CTSMA is essential.

III. Proposed Solution

The proposed CTSMA framework leverages the correlation properties of ZCZ signals but encounters challenges when using homogeneous ZCZ sequences (present in different cyclic time shifts) in a UAC network between multiple users. This is particularly evident in scenarios with unpredictable reflection and scattering, which can distort signals and lead to significant Multiple Access Interference (MAI) due to the zero correlation characteristic. Unlike CDMA, CTSMA is non-linear and non-coherent and does not need to insert pilot sequences for expensive coherent detection or channel estimation. Specifically, the CTSMA framework aims to identify multiple ZCZ sequences that maintain specific properties: (i) low auto-correlation except at zero time shift, (ii) low cross-correlation with other signals in the network, and (iii) similar transmission power to minimize interference among users. Two crucial metrics for evaluating the CTSMA sequences are the Periodic Auto-Correlation (PAC) and Periodic Cross-Correlation (PCC) features. The ideal Periodic Auto-Correlation Function (PACF) mitigates Inter-Symbol Interference (ISI) caused by factors like multipath effects and additive noise in the PHY layer, while the Periodic Cross-Correlation Function (PCCF) addresses interference among users in the MAC layer. The proposed CTSMA scheme aims to integrate these features to achieve robustness against both types of interference.

Code Division of CTSMA: Inspired by *Zadoff-Chu Sequence*, a variation sequence is used in the CTSMA system. Let $\boldsymbol{\alpha}_n$ be the code sequence assigned to a user denoted by α in the network,

$$\boldsymbol{\alpha}_n^{(k)} = \exp[\frac{k\pi\sqrt{-1}(n^2+n)}{N}],\ n = 0, 1, ..., N-1, \quad (1)$$

where $N \equiv 1 \pmod 2$ is the length of $\boldsymbol{\alpha}_n$, and it is decided by the number of users within a network. $k < N$ is the code identification coefficient for such a user, which is identity and pre-assigned. Another user in the same network denoted by β will be assigned another unique code $\boldsymbol{\beta}_n$ with identification coefficient l and which,

$$\boldsymbol{\beta}_n^{(l)} = \exp[\frac{l\pi\sqrt{-1}(n^2+n)}{N}],\ n = 0, 1, ..., N-1. \quad (2)$$

Note that the maximum number of users within a network is determined by N, with some mathematical restrictions, and will be discussed in this section. The PACF of each user's CTSMA sequence is ideal, i.e., the PACF of user α has the form,

$$R_{k,k}(m) = \frac{1}{N}\sum_{i=0}^{N-1} \boldsymbol{\alpha}_n^{(k)}[i] \cdot \overline{\boldsymbol{\alpha}_{n+m}^{(k)}[i]} = \delta[m], \quad (3)$$

where $m = 0, 1, ..., N-1$ is cyclic time shift. $\overline{[\cdot]}$ is the complex conjugate value. $\delta[m]$ represents Kronecker delta function which depicts the autocorrelation function $R_{k,k}(m)$ in the cyclic time shift perspective. The PACF of user β, $R_{l,l}(m)$, has the same behavior as the first. The predefined code coefficient assigned to different users is determined by the following conditions, let c be the set of all the possible coefficients in a single network:

$$k, l, ... \in c, \quad s.t.\ \gcd(k, N) = 1,\ \gcd(k-l, N) = 1, \quad (4)$$

where $\gcd()$ denotes greatest common divisor [34]. In other words, each coefficient must be mutually prime with N, as

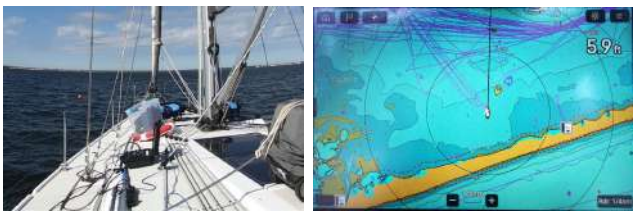

(a) (b)

Fig. 2: (a) A photograph captured from the deck of the vessel we used during the at-sea experiment. (b) Navigation system from the boat, which indicated our location during the channel information acquisition experiment in Barnegat Bay, NJ. Based on the distance scale indicator shown on the screen, we are around 1 nautical mile away from the land.

well as the difference between any two coefficients. The PCCF between two users, that is, user α with coefficient k and user β with coefficient l would have such a correlation function:

$$R_{k,l}(m) = \frac{1}{N}\sum_{i=0}^{N-1} \boldsymbol{\alpha}_n^{(k)}[i] \cdot \overline{\boldsymbol{\beta}_{n+m}^{(l)}[i]} = \frac{1}{\sqrt{N}}, \tag{5}$$

Although the cross-correlation is not ideal ($\neq 0$), the relatively low result is still eligible to ensure robustness when multiple signals are overlapped or intersected.

Transmitter: Considering these conditions, a trade-off between transmission efficiency and robustness is leveraged to determine the optimal value of N for the N-ary CTSMA scheme. The host, typically a floating buoy in underwater IoT, will compute and assign the identity coefficients to each user on the network. In each frame, $K = \log_2(N)$ data bits are encoded from binary to decimal numbers, denoted as D, where $D \in [1, N]$, and hence perform cyclic convolution with the corresponding CTSMA sequence. For each frame, modulated symbol $\mathbf{x}^{(\alpha)}$ can be computed:

$$\mathbf{d}^{\alpha}[n] = \delta\left[(n+D) \mod N\right] \tag{6a}$$

$$\mathbf{x}^{(\alpha)} = \boldsymbol{\alpha}_n^{(k)} \cdot \mathbf{d}^{\alpha}[n] = (\boldsymbol{\alpha} \circledast \mathbf{d})[n] \tag{6b}$$

where $\mathbf{d}^{\alpha}[n]$ is the cyclic impulse sequence with impulse emerges in cyclic time shift $n = -D \mod N$. $\boldsymbol{\alpha}_n^{(k)}$ is the code sequence for the user α. $n, m = 0, 1, ..., N-1$ represents the position and every cyclic time shift of the sequence, and "$\circledast$" denotes the cyclic convolution operator. The modulated symbols would preserve fine autocorrelation and cross-correlation in multiple access circumstances. The constant amplitude characteristic is essential to increase power efficiency, especially in underwater IoT devices, in which front-end amplifiers are highly power-limited.

Receiver: The demodulator in the receiver, assume the user i.e. $\hat{\alpha}$, intends to demodulate and decode the transmitted signal $\boldsymbol{\alpha}_n$ from the received signal. Let $\mathbf{y}$ be the received signal, which is contaminated with multiple different CTSM signals (recognized as interference) with various time delays, as well as the additive noise, as follows:

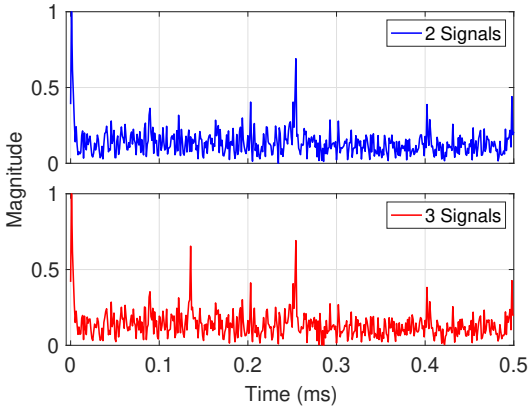

Fig. 3: Cross-correlation detection in the receiver based on the real collected channels in the at-sea experiment: Two coexistence signals and three coexistence signals.

$$\mathbf{y} = \mathbf{x}^{(\alpha)} * \mathbf{h}^{(\alpha)} + \mathbf{x}^{(\beta)} * \mathbf{h}^{(\beta)} + \cdots + \boldsymbol{\sigma} \tag{7}$$

where "$*$" denotes convolution. $\mathbf{h} = [h_0, h_1, h_2, ...]$ is the channel response to each link. $\boldsymbol{\sigma}$ is the additive noise.

The receiver $\hat{\alpha}$ can demodulate transmitted signal $\boldsymbol{\alpha}_n$ by constructing a demodulation matrix $\mathbf{A}$:

$$\mathbf{A} = \begin{bmatrix} \overline{\alpha_0^{(k)}} & \overline{\alpha_1^{(k)}} & \cdots & \overline{\alpha_{N-1}^{(k)}} \\ \overline{\alpha_{N-1}^{(k)}} & \overline{\alpha_0^{(k)}} & \cdots & \overline{\alpha_{N-2}^{(k)}} \\ \vdots & \vdots & \ddots & \vdots \\ \overline{\alpha_1^{(k)}} & \overline{\alpha_2^{(k)}} & \cdots & \overline{\alpha_0^{(k)}} \end{bmatrix} \tag{8}$$

where the matrix $\mathbf{A}$ is the stack of the demodulation code $\overline{\boldsymbol{\alpha}_n}$ of every copy of the cyclic time shift. The impulse response sequence $\hat{\mathbf{d}}^{\hat{\alpha}}[n]$ can be obtained by the cyclic position when detecting the peak among the channel impulse response $\mathbf{h}$, which can be computed by PCCF:

$$\hat{\mathbf{d}}^{\alpha}[n] = \max\{h_0, h_1, \ldots, h_{N-1}\} = \max\{\frac{1}{N}(\mathbf{y} \circledast \mathbf{A})\}, \tag{9}$$

where h_n is the channel impulse response in $\mathbf{h}$. The decimal number D can be reached by the position index of the peak within the channel response. M length binary bits can be decoded by the decimal-to-binary ratio of D. Although the orthogonality between the correct signal and other interference signals is not perfect, the cross-correlation between two sequences ($\frac{1}{\sqrt{N}}$ calculated in (5)) is relatively low, hence guaranteeing the noise reduction capability of this demodulator. The CTSMA encoding rate can be calculated by $M/2^M$, where M denotes the modulation order of CTSMA.

IV. Performance Evaluation

To validate our proposed solution, we conducted emulations with real underwater acoustic channels, which were collected

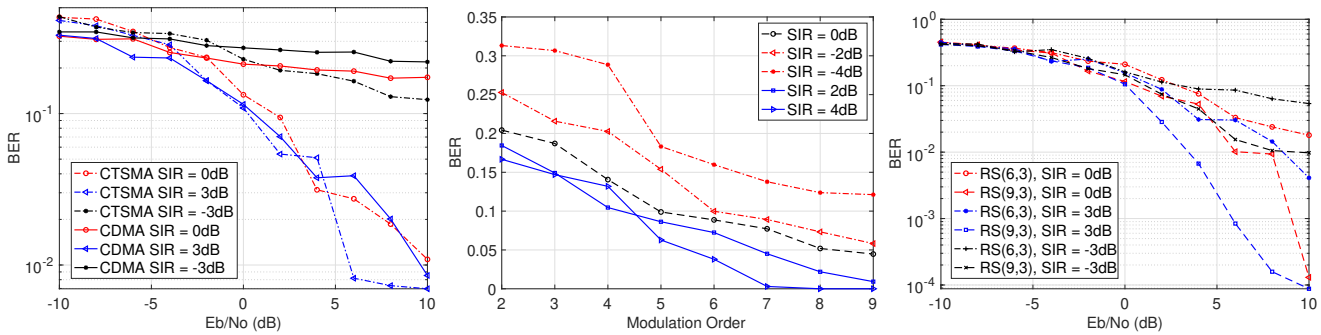

Fig. 4: (a) The BER evaluation when 0.32 ms Cyclic Prefix (CP) is inserted, with varying Signal to Interference Ratio (SIR) for CTSMA and CDMA schemes. The modulation order is 5, the encoding rate is $5/32$. (b) CTSMA performance of varying modulation order against different levels of SIR, assumed the SNR of additive noise is 10 dB. (c) When CTSMA modulation order = 5, the performance enhancement evaluation based on two types of RS coding strategies with different SIR.

from at-sea experiments. The channel model is introduced in detail in Section IV-A. We also implement our proposed scheme with our custom-made underwater transceiver and obtain detailed results in real-time monitoring in Section IV-B.

A. *Emulations*

Emulation Setup: The proposed CTSMA transceiver system is emulated through MATLAB. CDMA scheme with the same encode rate is adopted as a baseline to assess our proposed solution. We use chaotic sequences in CDMA as spreading code, owing to its characteristics of nonlinearity and adaptation. As shown in Fig. 2, the underwater acoustic channels in the emulations were collected at Barnegat Bay, NJ, in May 2023; The water depth of this bay is around 3.35 m and the wind speed is approximately 15 kts. We used two SDR hardware Universal Software Radio Peripheral (USRP) X300 boards [35], with a transmission depth of 0.5 m and a transmission distance of 10 m. The center frequency is 100 kHz and the bandwidth is 100 kHz. The normalized Signal-to-Noise Ratio (SNR) is about 20 dB in terms of normalized SNR (Eb/No). Given that the proposed CTSMA is based on the CTSMA sequences mentioned above, we establish a comparative analysis of its performance across various modulation orders. This evaluation utilizes a metric involving chaotic code-based CDMA, alongside corresponding encoding rates. An Additive White Gaussian Noise (AWGN) with SNR varying from -10 dB to 10 dB is assumed to be noise due to energy-constrained front-end circuits in the transmitter and receiver. We emulate and compare the performance across varied parameters: (i) different modulation order M; (ii) different numbers and strength of concurrent transmissions; (iii) with and devoid of Cyclic Prefix (CP).

Emulation Results: Fig. 3 shows the channel information collected at the receiver from two scenarios we used in emulation: the upper one is the impulse response of two transmitters transmitting simultaneously and the lower one is which of three transmitters transmitting simultaneously. Note that all of these transmitters are assumed to transmit signals with the same power level. Except for the first LOS impulse, the interference impulses that exceed more than half of the LOS power level appeared in both figures, that is, because the periodic cross-correlation reference in (5) shows the result of $\frac{1}{\sqrt{N}}$. We collect the respective impulse response at modulation order $M = 3$, hence $N = 2^M = 8$, therefore the power level of interference should be around $\frac{1}{\sqrt{8}} \approx 0.354$. With the addition of the multipath effect, the interference impulse can reach 0.6 times the LOS power. When more than 1 interference signal appears, the receiver will not be able to detect the peak accurately if two or more interference impulses are in the same position, which will cause failed demodulation. Therefore, BER has a negative correlation with the increase in modulation order, depicted in the x-axis of Fig. 4(b). Fig. 4(a) depicts the performance of the CTSMA and CDMA schemes in terms of BER. In contrast to Fig. 5, we intend to discover the robustness against interference signals without the multipath effect. The multipath effect has a severe impact on performance, as the length of the multipath channel is much longer than the length of each transmitted frame. Therefore, a CP sequence with a length of 0.32 ms is added in front of each frame to reduce the ISI. When the strength of the interference signal, in terms of SIR, is 3 dB, both CTSMA and CDMA with the same encoding rate show their capability. However, when SIR = 0 dB, in which the interference signal has the same power level, the CTSMA scheme reveals better robustness compared to the CDMA scheme. Fig. 4(b) illustrates the performance of different modulation orders that ranged from 2 to 9 with five different levels of interference signal strength, as shown in the legend. BER achieves < 0.2 when the modulation order is greater than 5, even in the case of SIR = -4 dB, in which the strength of the interference signal is approximately 2.5 times stronger than the transmitted signal. Notice that no CP or channel coding is performed, where the CP (Fig. 4(a)) and channel coding (Fig. 4(c)) can significantly improve the decoding performance. Fig. 4(c) depicts the performance with

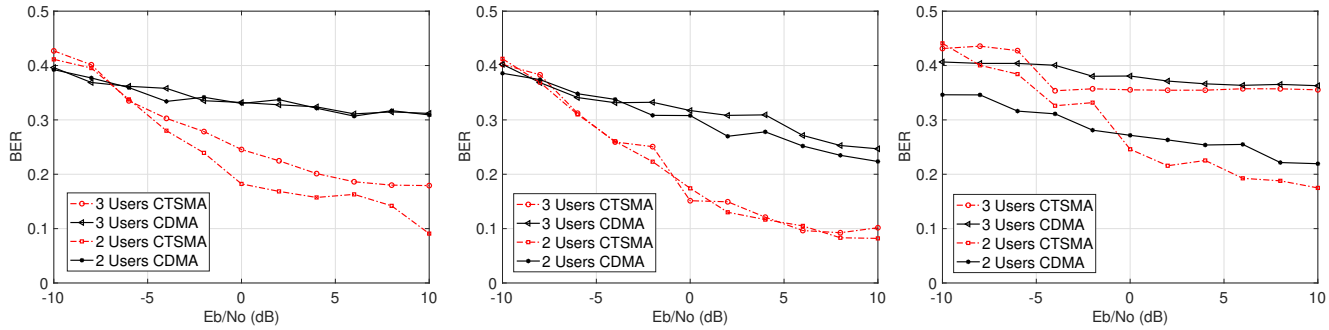

(a) (b) (c)

Fig. 5: When modulation order is 5, the BER versus normalized SNR (Eb/No) of different numbers of users with the interference signal strength of (a) SIR of each interference signal = 0 dB; (b) SIR of each interference signal = 3 dB; (c) SIR of each interference signal = -3 dB. CP is not added and is without channel coding.

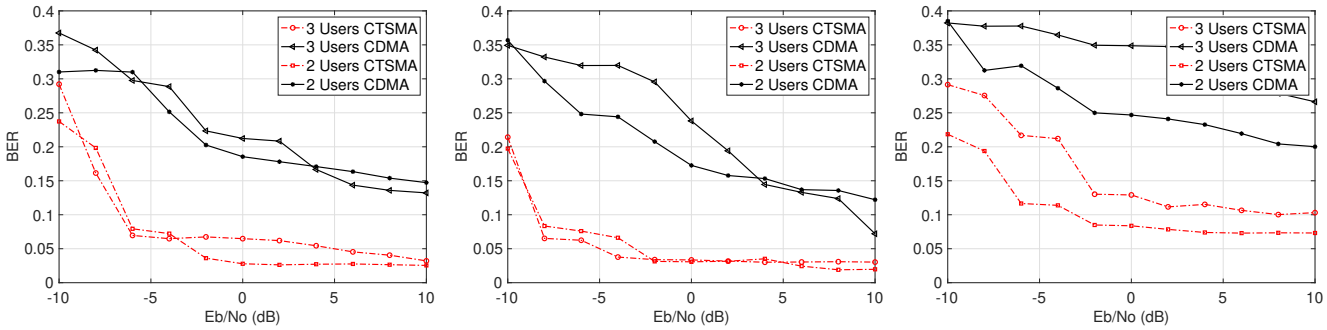

(a) (b) (c)

Fig. 6: When modulation order is 8, the BER versus normalized SNR (Eb/No) of different numbers of users with the interference signal strength of (a) SIR of each interference signal = 0 dB; (b) SIR of each interference signal = 3 dB; (c) SIR of each interference signal = -3 dB. CP is not added and is without channel coding.

the employment of channel coding. We use Reed-Solomon (RS) coding and two coding strategies are considered: RS(6,3) and RS(9,3). Different colors represent the various SIR values, and the style of the lines indicates the order of RS coding. More specifically, a high-order RS coding can compensate for the strong interference strength level: By comparing two curves (i) RS(9,3), SIR=-3 dB, and (ii) RS(6,3), SIR=3 dB, we notice that the higher order RS coding strategy is capable of counteracting SIR 6 dB at similar SNR levels. Therefore, it is worth considering the trade-off and adaptive switching when implementing the CTSMA scheme in different users and different distances (leading to different signal power).

We further analyze and discuss the following cases for both CTSMA and CDMA: (i) CTSMA modulation order = 5, where the corresponding encoding rate is $5/2^5 \approx 0.156$, and (ii) Modulation order = 8, where the corresponding encoding rate is $8/2^8 \approx 0.03$. We first analyze the performance as the modulation order = 5 is selected, since in this configuration the BER for all SIR environments has a notable descent according to Fig. 4(b). Fig. 5 shows a detailed illustration of the performance when there are 2 and 3 users within the network, with various SIR levels. Notice that the sum of two 0 dB SIR interference signals is not equivalent to a single -3 dB SIR interference signal, since the positions of the impulses are separated in the previous case, as suggested in Fig. 3. The impacts of the multipath effect are different. Therefore, it is necessary to evaluate both cases. However, due to the unpredictable multipath effect and Doppler effect, the adaptive use of CP and the choice of modulation order is dispensable in practice. In Figs. 5(a) and 5(b), we observe that the CTSMA scheme has much better resistance to interference signal than the chaotic code that we use in CDMA as a metric. As mentioned above, the use of CP and channel coding can provide significant enhancement, which we are realizing in the tank experiment. As shown in Fig. 5(c), in the scenario involving three users, both CTSMA and CDMA are unable to accurately demodulate the signal when the SIR for each interfering signal is -3 dB. We also notice that when additive noise is strong (Eb/No < -7 dB), the CDMA has a lower BER than the CTSMA scheme. Secondly, we select to evaluate the performance of CTSMA versus CDMA when the CTSMA modulation order is 8. The reason is that in this case, the

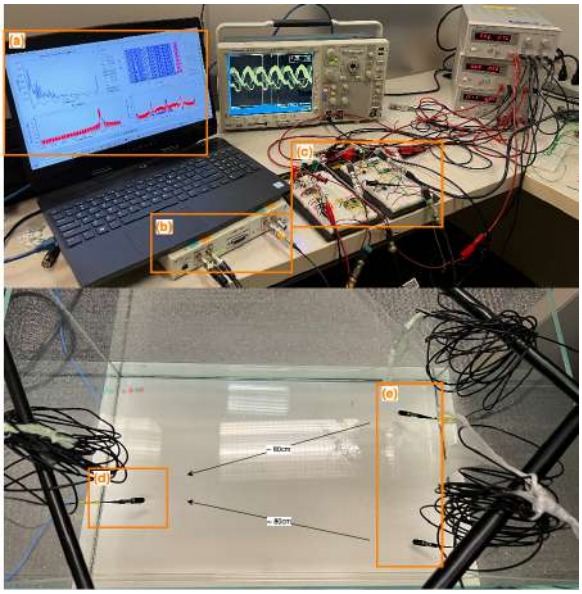

Fig. 7: Testbed for experiments: (a) GNU Radio Companion (GRC) in laptop; (b) USRP X300 board, with 2 Tx channels and 1 Rx channel; (c) Custom-made front-end circuits, with various amplifiers and filters; (d) A hydrophone as receiver; And (e) Two transducers as transmitters, where the distance from Tx to Rx is around 80 cm for both channels. The two electronic devices on the table are the oscilloscope (middle) used to monitor the strength and shape of the signal waveform and the Direct Current (DC) power supplies (right) used to provide power and control the voltage-controlled Variable Gain Amplifier (VGA) in the front-end circuits.

length of the CTSMA sequence is long enough to resist most of the multipath effect in application scenarios, including the emulation channel and the tank experiment channel. With the comparison to previous results (Fig. 5, modulation order = 5), we observe that the BER performance of the CTSMA scheme is more sensitive to the increase in the length of the CTSMA sequence than CDMA. Especially in a strong interference situation (depicted in Fig. 6(c)), both CTSMA cases achieve much lower BER than CDMA in the same metrics, that is because the value of PCCF went down as the elevated length of the CTSMA sequence.

B. Tank Experiments

Experiment Testbed: Based on the multi-transducer water tank experiments and online signal monitoring testbed, we intend to validate that our proposed CTSMA scheme is practicable. Considering the limited size of the water tank (0.8 m $\times$ 0.4 m) and the shallow depth (10 cm), the channel condition is actually inferior to open-underwater space conditions, such as an ocean with deep depth. The strength of the multipath effect is extreme due to the reflection and scattering of the acoustic wave. To counteract the multipath effect, we set the modulation

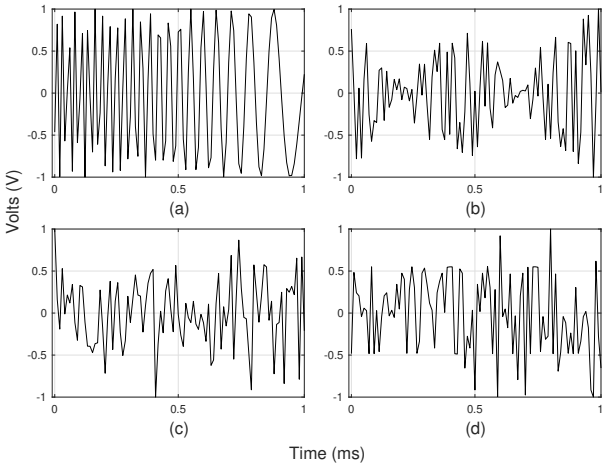

Fig. 8: Various time domain transmitting signals delivered by USRP in 1 ms intervals, their corresponding PAPR has also been evaluated: (a) CTSMA, PAPR $= 3.05$ dB; (b) QAM-modulated CDMA, PAPR $= 7.21$ dB; (c) OFDM, PAPR $= 8.07$ dB; (d) OSDM, PAPR $= 6.82$ dB.

order to 8, where the modulation order of 5 is adequate in most application scenarios. As shown in Fig. 7, two transducers are placed in the tank and the signal is transmitted simultaneously with assigned CTSMA sequences in different coefficients, as mentioned in Section III. The distance between transducers is approximately 40 cm and the transmission distance is around 80 cm. The front-end circuits are designed for IoT devices, therefore the view of Printed Circuit Boards (PCB) is shown in Fig. 1. The size is around 10 cm $\times$ 5 cm and the total power consumption is 1.7 W, where 1.2 W for the transmitter and 0.5 W for the receiver. The omnidirectional transducers and hydrophone we use in our testbed are Teledyne RESON TC4013, with a transmitting sensitivity of 130 dB re 1 μPa/V at 1 m at 100 kHz and a receiving sensitivity of -211 dB re 1 μPa/V [36]. The optimal operation frequency band range is between 50 kHz and 150 kHz.

Constant Amplitude: To adapt the power-constrained modem in IoT devices, especially the linear Op-Amp and limited power filters, the characteristic of constant amplitude (CA) is indispensable. Firstly, a CA modulation can maximize the efficiency and hence increase the SNR. Secondly, some linear electronic components such as Op-Amp and transistors used in various types of filters may be damaged if the input voltage strength exceeds the limitation at any moment. Fig. 8 shows the amplitude of the transmit signals in Volts and the spectrum density generated by the proposed CTSMA frameworks versus multiple existing schemes, including QAM-modulated CDMA, OFDM, and OSDM. To adapt the configuration of amplifiers in our front-end circuit, we normalize every transmit signal to 2 Vpp with 0 V offset. Based on the time-domain transmitting signal of each scheme, we notice that the CTSMA signal

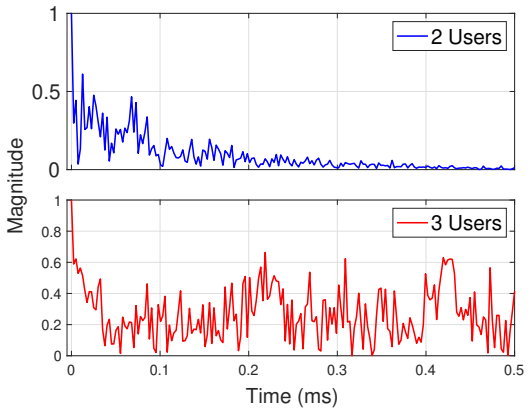

Fig. 9: Cross-correlation response collected in the water tank. The upper one is when only two users are within the network: one transmit and one receive, which LOS has twice as much receive power as the rest multipath paths. The lower one is when two transmitters transmit equivalent transmit power CTSMA signals simultaneously and this impulse response is detected and generated in the receiver.

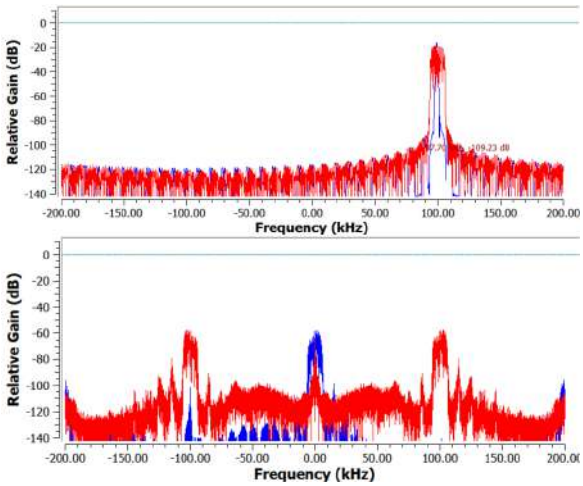

Fig. 10: Signal monitoring from GRC by using USRP in water tank experiment. The upper one is the transmission signals from two separated transmitters (shown in Red and Blue colors), with the intention of evaluating a multiuser communication network system. The lower one is the received signal extracted from the receiver, with the Passband in red color and the Baseband in blue color.

is eligible to achieve substantially lower PAPR, which leads to significant advantages in both power amplifier efficiency and robustness against non-linear distortion. In the other three schemes (Fig. 8(b)-(d)), the transmitted signal must be strictly normalized, leading to spectrum wasting. However, the CA feature of CTSMA ensures the maximum usage of the entire spectrum. In addition, the feature of CA in underwater IoT devices promotes the longevity and durability of the hardware by avoiding the peaks in power demand that typically strain electronic components. This is particularly beneficial in the underwater context where maintenance and replacement of components can be logistically challenging and expensive. In addition, the adoption of CA modulation helps reduce the overall power consumption of the communication system, which is a critical advantage given the limited energy resources available in underwater settings.

Experiment Results: We investigate the feasibility of our proposed CTSMA scheme based on the testbed shown in Fig. 7. Two transducers (acting as transmitters) are placed on one side of the water tank, and one hydrophone (acting as receiver) is placed on the other side. In this experiment, the center frequency is 100 kHz and the bandwidth is 10 kHz. We evaluate the multipath condition of the channel by comparing the collected channel impulse responses of (i) only one transmitter is transmitting, and (ii) both transmitters are transmitting at the same power level (Fig. 9). In the one-link scenario, the channel has a multipath delay time of approximately 0.1 ms, with around 10 taps. Most of these taps are produced from signal reflections, i.e., the surface of the water, the walls, and the bottom of the water tank. The BER can achieve $10^{-3.6} \approx 0.00025$ in this case. In contrast, the lower impulse response diagram in Fig. 9 is collected in the receiver when two transducers transmit signals simultaneously using the proposed CTSMA method with equivalent power levels. In addition to reflections similar to the previous scenario, we can clearly see that the Signal to Interference and Noise Ratio (SINR) is reaching 3 dB during 0.2 ms to 0.5 ms, attributable to the other transducer. As discussed in equation ((5)), the cross-correlation between two transmit signals can be calculated $R_{k,l} = \frac{1}{\sqrt{N}}$, plus the addition of other multipath effects, so the impulses appeared with some delays. However, LOS is still detectable and therefore BER can be assured around $10^{-3} = 0.001$, before forward error control (FEC) is applied. Fig. 10 shows the frequency domain information of the monitored baseband and passband signals from the transmitter and receiver; We choose a Root Raised Cosine (RRC) filter with a roll-off factor $\beta = 0.35$ to reduce Intersymbol Interference (ISI) in this experiment circumstance.

V. Conclusions

To achieve a reliable and efficient underwater acoustic communication of the UnderWater Internet of Things (UW IoT), we proposed a novel strategy that integrates the Physical (PHY) layer and Medium Access Control (MAC) layer technology, called Cyclic Time Shift Multiple Access (CTSMA). The concept of the proposed method is leveraging the auto-correlation and cross-correlation properties of multiple CTSMA sequences to assign them to various users in a communication network, enabling simultaneous signal transmission. We evaluated the performances by validating through emulation based on real

channels collected in the at-sea experiment and our custom-made tank experiment testbed.

Future Work: Given the awareness that our tank experiment is insufficient due to the limited size of the water tank, our next goal is to proceed our scheme to the pool experiment and further to the lake/sea experiment. Therefore, the practicality of our proposed scheme can be proved and more valuable information can be collected. Furthermore, the trade-off between the various user numbers within the network and their corresponding performance will be examined through the development of an enhanced emulator.

Acknowledgement: This work was supported by the NSF NeTS Award No. CNS-1763964.

REFERENCES

[1] D. Pompili and I. F. Akyildiz, "Overview of networking protocols for underwater wireless communications," *IEEE Communications Magazine*, vol. 47, no. 1, pp. 97–102, 2009.

[2] D. C. Nguyen, M. Ding, P. N. Pathirana, A. Seneviratne, J. Li, D. Niyato, O. Dobre, and H. V. Poor, "6G Internet of Things: A comprehensive survey," *IEEE Internet of Things Journal*, vol. 9, no. 1, pp. 359–383, 2022.

[3] S. Huang, C. Sun, R.-Q. Wang, and D. Pompili, "Multi-behavior multi-agent reinforcement learning for informed search via offline training," *20th International Conference on Distributed Computing in Smart Systems and the Internet of Things (DCOSS-IoT)*, pp. 1–8, 2024.

[4] K. Anjum, Z. Li, and D. Pompili, "Acoustic channel-aware autoencoder-based compression for underwater image transmission," in *2022 Sixth Underwater Communications and Networking Conference (UComms)*, 2022, pp. 1–5.

[5] Z. Qi, X. Zhao, and D. Pompili, "Polarized OFDM-based pulse position modulation for high-speed wireless optical underwater communications," in *IEEE Transactions on Communications*, vol. 71, no. 12, 2023, pp. 7163–7173.

[6] X. Zhao, Z. Qi, and D. Pompili, "Link adaptation in underwater wireless optical communications based on deep learning," *Computer Networks*, vol. 242, pp. 1–11, 2024.

[7] Y.-T. Hsieh, Z. Qi, and D. Pompili, "Full-duplex underwater acoustic communications via self-interference cancellation in space," *Journal of Communications and Networks*, vol. 25, no. 2, pp. 167–181, 2023.

[8] A. Palmeiro, M. Martín, I. Crowther, and M. Rhodes, "Underwater radio frequency communications," in *OCEANS 2011 IEEE - Spain*, 2011, pp. 1–8.

[9] I. F. Akyildiz, D. Pompili, and T. Melodia, "Underwater acoustic sensor networks: research challenges," *Ad Hoc Networks*, vol. 3, no. 3, pp. 257–279, 2005.

[10] D. Pompili, T. Melodia, and I. F. Akyildiz, "Three-dimensional and two-dimensional deployment analysis for underwater acoustic sensor networks," in *Ad Hoc Networks*, vol. 7, no. 4, 2009, pp. 778 – 790.

[11] M. C. Domingo, "An Overview of the Internet of Underwater Things," *Journal of Network and Computer Applications*, vol. 35, no. 6, pp. 1879–1890, 2012.

[12] Z. Fang, J. Wang, C. Jiang, Q. Zhang, and Y. Ren, "AoI-inspired collaborative information collection for AUV-assisted internet of underwater things," *IEEE Internet of Things Journal*, vol. 8, no. 19, pp. 14 559–14 571, 2021.

[13] J. Xu, M. A. Kishk, and M.-S. Alouini, "Coverage enhancement of underwater Internet of Things using multilevel acoustic communication networks," *IEEE Internet of Things Journal*, vol. 9, no. 24, pp. 25 373–25 385, 2022.

[14] A. Babić, F. Ferreira, N. Kapetanović, N. Mišković, M. Bibuli, G. Bruzzone, C. Motta, R. Ferretti, A. Odetti, M. Caccia, S. Aracri, and F. De Pascalis, "Cooperative marine litter detection and environmental monitoring using heterogeneous robotic agents," in *OCEANS 2023 - Limerick*, 2023, pp. 1–6.

[15] V. Sadhu, Z. Li, Z. Qi, and D. Pompili, "High-resolution data acquisition and joint source-channel coding in underwater IoT," *IEEE Internet of Things Journal*, vol. 10, no. 16, pp. 14 003–14 013, 2023.

[16] V. Sadhu, M. Rahmati, and D. Pompili, "Mosfet-based ultra-low-power realization of analog joint source-channel coding for IoTs," in *2019 16th Annual IEEE International Conference on Sensing, Communication, and Networking (SECON)*, 2019, pp. 1–3.

[17] M. Rahmati, D. Pompili, and R. Petroccia, "Collaborative hybrid arq for CDMA-based reliable underwater acoustic communications," in *2018 Fourth Underwater Communications and Networking Conference (UComms)*, 2018, pp. 1–5.

[18] S. Hussain and S. Barton, "Comparison of coherent and non-coherent modulation schemes for low-data rate hand-held satellite terminals subject to high phase noise," in *1995 Tenth International Conference on Digital Satellite Communications*, 1995, pp. 339–342 vol.1.

[19] H. Sari and B. Woodward, "Underwater acoustic voice communications using digital pulse position modulation," in *Oceans '97. MTS/IEEE Conference Proceedings*, vol. 2, 1997, pp. 870–874 vol.2.

[20] H. Kulhandjian and T. Melodia, "Modeling underwater acoustic channels in short-range shallow water environments," in *WUWNet '14: Proceedings of the 9th International Conference on Underwater Networks & Systems*. New York, NY, USA: Association for Computing Machinery, 2014.

[21] A. Mahmood and M. Chitre, "Detecting OSDM signals in sparse channels and snapping shrimp noise," in *2018 Fourth Underwater Communications and Networking Conference (UComms)*, 2018, pp. 1–5.

[22] Z. Qi and D. Pompili, "UW-CTSM: Circular time shift modulation for underwater acoustic communications," in *2022 17th Wireless On-Demand Network Systems and Services Conference (WONS)*, 2022, pp. 1–8.

[23] Z. Qi and D. Pompili, "Circular time shift modulation for robust underwater acoustic communications in doubly spread channels," in *Computer Communications*, vol. 207, 2023, pp. 77–85.

[24] N. Chirdchoo, W.-S. Soh, and K. C. Chua, "Aloha-based MAC protocols with collision avoidance for underwater acoustic networks," in *IEEE INFOCOM 2007 - 26th IEEE International Conference on Computer Communications*, 2007, pp. 2271–2275.

[25] N. Morozs, P. Mitchell, and Y. V. Zakharov, "TDA-MAC: TDMA without clock synchronization in underwater acoustic networks," *IEEE Access*, vol. 6, pp. 1091–1108, 2018.

[26] X. Cheng, F. Qu, and L. Yang, "Single carrier FDMA over underwater acoustic channels," in *2011 6th International ICST Conference on Communications and Networking in China (CHINACOM)*, 2011, pp. 1052–1057.

[27] R. Doost-Mohammady, M. Y. Naderi, and K. R. Chowdhury, "Performance analysis of CSMA/CA based medium access in full duplex wireless communications," *IEEE Transactions on Mobile Computing*, vol. 15, no. 6, pp. 1457–1470, 2016.

[28] S. Yang, *OFDMA System Analysis and Design*, ser. Artech House mobile communications library. Artech House, 2010. [Online]. Available: https://books.google.com/books?id=UcJPmAEACAAJ

[29] D. Pompili, T. Melodia, and I. F. Akyildiz, "A CDMA-based medium access control for underwater acoustic sensor networks," *IEEE Transactions on Wireless Communications*, vol. 8, no. 4, pp. 1899–1909, 2009.

[30] M. Rahmati, R. Petroccia, and D. Pompili, "In-network collaboration for CDMA-based reliable underwater acoustic communications," *IEEE Journal of Oceanic Engineering*, vol. 44, no. 4, pp. 881–894, 2019.

[31] M. Rahmati, Z. Qi, and D. Pompili, "Underwater adaptive video transmissions using mimo-based software-defined acoustic modems," *IEEE Transactions on Multimedia*, vol. 25, pp. 473–485, 2023.

[32] Z. Qi, R. Petroccia, and D. Pompili, "ASVTuw: Adaptive scalable video transmission in underwater acoustic multicast networks," in *Proceedings of the 16th International Conference on Underwater Networks & Systems*, ser. WUWNet '22. New York, NY, USA: Association for Computing Machinery, 2022. [Online]. Available: https://doi.org/10.1145/3567600.3568137

[33] Z. Qi, Z. Li, and D. Pompili, "Orthogonal signal division multiple access for multiuser underwater acoustic networks," in *2023 IEEE 20th International Conference on Mobile Ad Hoc and Smart Systems (MASS)*, 2023, pp. 390–396.

[34] H.-J. Zepernick and A. Finger, *Nonbinary Pseudo Random Sequences*. John Wiley & Sons, Ltd, 2005, ch. 5, pp. 127–172. [Online]. Available: https://onlinelibrary.wiley.com/doi/abs/10.1002/9780470866597.ch5

[35] "USRP X Series," https://www.ettus.com, 2023, accessed Apr 20, 2023.

[36] "RESON TC4013 Hydrophone Product Information," http://www.teledynemarine.com/reson-tc4013, 2023, accessed Apr 20, 2023.